PLOS ONE

RESEARCH ARTICLE

The impact of anions on electrooxidation of perfluoroalkyl acids by porous Magnéli phase titanium suboxide anodes

Yaye Wang[1,2], Yifei Wang[2], Shuping Dong[2], Qingguo Huang[2]*

1 Jiangsu Provincial Academy of Environmental Science, State Environmental Protection Key Laboratory of Aquatic Ecosystem Health in the Middle and Lower Reaches of Yangtze River, Nanjing, People's Republic of China, **2** Department of Crop and Soil Sciences, College of Agricultural and Environmental Sciences, University of Georgia, Griffin, Georgia, United States of America

* qhuang@uga.edu

Citation: Wang Y, Wang Y, Dong S, Huang Q (2025) The impact of anions on electrooxidation of perfluoroalkyl acids by porous Magnéli phase titanium suboxide anodes. PLoS ONE 20(1): e0317696. https://doi.org/10.1371/journal.pone.0317696

Editor: Ivan P. Kozyatnyk, Linköping University: Linkopings universitet, SWEDEN

Received: August 25, 2024

Accepted: January 2, 2025

Published: January 23, 2025

Data Availability Statement: All relevant data are within the manuscript and its Supporting Information files.

Funding: This study was supported in part by U.S. Department of Defense SERDP ER-2717, ER-1320 and U.S. Environmental Protection Agency Grant R84008001.

Competing interests: A patent is awarded on "Methods and Systems for Electrochemical Oxidation of Polyfluoroalkyl and Perfluoroalkyl

Abstract

Previous studies have indicated the great performance of electrooxidation (EO) to mineralize per- and polyfluoroalkyl substances (PFASs) in water, but different anions presented in wastewater may affect the implementation of EO treatment in field applications. This study invetigated EO treatment of perfluorooctane sulfonate (PFOS) and perfluorooctanoic acid (PFOA), two representative perfluoroalkyl acids (PFAAs), using porous Magnéli phase titanium suboxide anodes in electrolyte solutions with different anions present, including NO_3^-, SO_4^{2-}, CO_3^{2-} and PO_4^{3-}. The experiment results indicate that CO_3^{2-} enhanced PFAS degradation, while NO_3^- suppressed the degradation reactions with its concentration higher than 10 mM. SO_4^{2-} and PO_4^{3-} exhibited less impact. Further studies with electrochemical characterizations and radical quenching experiments illustrate the mechanisms of how the anions may impact EO performance.

Introduction

Per- and polyfluoroalkyl substances (PFASs) constitutes a large family of human-made chemicals that have developed for a few decades, comprising at least one perfluoroalkyl moiety,–C_nF_{2n}– [1, 2], with perfluorooctanoic acid (PFOA) and perfluorooctane sulfonate (PFOS) being the most well-known species. Due to extensive application and unregulated disposal, PFASs can be detected in almost all environment media, including air [3], soil [4–7], groundwater [8–10] and even drinking water [11, 12]. PFASs are thermally and chemically stable with low reactivity, leading to their global distribution and accumulation [11, 13]. However, PFASs are shown closely correlated with numerous adversary health effect, including increased liver enzymes and cholesterol [14, 15], decreased birth weight and fetal growth [16, 17], and even kidney and testicular cancer [18, 19]. Due to their extensively existence, environmental persistence and potential carcinogenicity and toxicity, PFASs raises public concern since early 2000s. US Environmental Protection Agency has recently announced the enforceable levels of 4.0 ppt for PFOA and PFOS individually in drinking water [20].

Contaminants" (US11,512,011B2) with QH as one of the inventors.

The stability of PFASs and their surfactant nature make them highly resistant to many treatment technologies, such as advanced oxidation processes (AOPs), because hydroxyl free radicals ($HO^{\cdot}$) cannot effectively attack C-F bonds [21–23]. Numerous destructive technologies are being developed in order to fully mineralize PFASs, including photochemical oxidation [24, 25], sonochemical treatment [8, 26], plasma-based technology [27, 28], alkaline hydrothermal treatment [29, 30] and advanced reduction processes [31–33]. These destructive technologies are however still under development at different phases, suffering various limitations in terms of energy efficiency and demanding conditions. For example, the electrical energy necessary to reduce 90% PFOS(EE/O) for photochemical oxidation, plasma-based technology, and electron beam treatment were reported to be 122.22 $kWh{\cdot}m^{-3}$, 23.2 $kWh{\cdot}m^{-3}$ and 102–193 $kWh{\cdot}m^{-3}$, respectively [24, 27, 34]. Biodegradation was also shown effectiveness in PFAS removal [35–37], with up to 60% PFOA and PFOS removal reported for an enrichment culture of *Acidimicrobium* sp. strain A6 after 100 days of incubation, forming shorter-chain PFASs and fluoride ion as the intermediate products. 6:2 fluorotelomer sulfonate (6:2 FTS) was found to biotransform to PFPeA, PFHxA, and 5:3 Acid in aerobic sediments, while did not biodegrade under aerobic conditions.

Electrooxidation (EO) treatment is a promising wastewater treatment technology to destruct recalcitrant organic contaminants under ambient temperature and pressure [38–40]. EO occurs via anodic oxidation to degrade PFASs, primarily by direct electron transfer (DET) [41–43] with reactive oxygen species (ROS) also playing a role to facilitate the process [44, 45]. Both anode materials and water matrix may affect the performance of EO on PFASs degradation. The observed reaction rate constant normalized by geometric surface area of PFOS (k'_{SA}) were 2.06×10^{-5} $m{\bullet}s^{-1}$, 8.48×10^{-6} $m{\bullet}s^{-1}$ and 8.40×10^{-6} $m{\bullet}s^{-1}$ on Ti/TiO_2-NTs/Ag_2O/PbO_2, Ti/PbO_2 and Ti/TiO_2-NTs/PbO_2 anodes, respectively, when the current density was 30 $mA{\bullet}cm^{-2}$ [46]. For BDD and Si/BDD anodes, the k'_{SA} of PFOS degradation were 2.19×10^{-6} $m{\bullet}s^{-1}$ and 2.80×10^{-5} $m{\bullet}s^{-1}$, when the current densities were 15 $mA{\bullet}cm^{-2}$ and 23.24 $mA{\bullet}cm^{-2}$, respectively [47, 48]. Porous Magnéli phase Ti_4O_7 material exhibits high conductivity and electrocatalytic reactivity, chemical and thermal stability, long performance life and high oxygen evolution potential (OEP), thus making a promising candidate for electrochemical oxidation of PFASs as anode [49–51]. Since Ti_4O_7 anodes have porous structure, more electroactive sites are available for electrochemical reaction to take place. 99.5% PFOA and 93.1% PFOS were degraded on Ti_4O_7 anodes after 180 min EO reaction at 2.7 V vs. SHE in spiked water with 0.5 mM PFOA and 0.1 mM PFOS as initial concentrations using 20 mM $NaClO_4$ as supporting electrolytes [52]. However, natural waters commonly have different anions present, such as CO_3^{2-}, SO_4^{2-}, NO_3^{-} and PO_4^{3-}, which may compete with PFASs for the active sites on anode, while their effects on PFASs degradation during EO treatment have not been systematically examined.

Higher temperature was proved to favor the degradation of PFOA, with the removal rate increased from 83.3% to 90.7% after 30 min of EO treatment at 10 $mA{\cdot}cm^{-2}$ when the temperature increased from 10˚C to 22˚C [53]. However, the presence of other organic pollutants, such as trichloroethylene (TCE), apparently inhibited the degradation of PFOS [54]. There was still a lack of a systematic evaluation of the effect of different anions on PFAS degradation. This study aims to explore the effects of nitrate, sulfate, carbonate and phosphate ions on the degradation of PFOA and PFOS as model PFAS in water during EO with Ti_4O_7 anode. These anions are common in surface water and industrial wastewater. Spectroscopic and electrochemical characterizations were employed to elucidate the mechanisms underlying the effect of different anions. The results of this study provide useful information to guide the implementation of Ti_4O_7-based EO treatment for PFAS removal in contaminated waters or concentrated waste streams.

Materials and methods

Chemicals and reagents

The chemicals and reagents involved in this work were provided in the supporting information (S1 Text in S1 File) in detail.

Anode fabrication and characterization

The process of Ti_4O_7 fabrication was described in our previous study [45]. In brief, the Ti_4O_7 powders were obtained by reducing TiO_2 powder at 950˚C in H_2 atmosphere. The Ti_4O_7 powder was then pressed in the mold to form a green body. During this process, polyacrylamide/polyvinyl alcohol (95/5, m/m) was used as the binder to help molding. Finally the green body was further heated to 1350˚C and maintained at 1350˚C to form a bulk electrode. Vacuum is required during the whole sintering process. The dimension of the Ti_4O_7 anode used in this study was 70 mm in length, 45 mm in width, and 2.5 mm in thickness. The weight of the anode is 81.5 g.

The physical properties of the Ti_4O_7 anode were characterized by a number of techniques, such as XPert PRO MRD X-ray diffractometer (XRD) with CuKα1 radiation at 45kV/40mA (PAnalytical, Netherland) over the 2-Theta range of 10–80˚. The morphology is observed by Hitachi SU-8230 Scanning electron microscopy (SEM) (Schaumburg, USA). MicroActive AutoPore V 9600 (Norcross, GA) was used to characterize the size and volume of pores in the anode. Electrochemical characterizations including anodic potential (AP) measurement, linear sweep voltammetry (LSV) and cyclic voltammetry (CV) were performed on a CHI-660E electrochemical workstation (Austin, TX) with a leak-free Ag/AgCl reference electrode (CH Instrument). All anodic potentials in the study have been corrected with internal resistance (iR) compension and reported against hydrogen electrode (SHE).

Electrooxidation experiments

The experiments using spiked reaction solution were conducted in a self-designed acrylic batch reactor (6.50 cm×5.50 cm×5.70 cm) with the Ti_4O_7 plate as the anode. The volume of reaction solution is 100 mL throughout the study. 316 stainless steel plate was used as the cathode. The anode and cathode were in parallel placement and the distance between them was fixed at 2.5 cm. Constant current was supplied by a DC power source (Tacklife Inc, China). The initial concentration of PFOS and PFOA were 2.0 μM for each, and the supporting electrolytes is 100 mM $NaClO_4$. Sodium salts, $NaNO_3$, Na_2SO_4, Na_2CO_3 and Na_3PO_4, were added into the reaction solution at 1.0, 5.0, 10 or 20 mM to assess the effect of different anions on PFOS degradation. Duplicate 400 μL samples were collected at each predetermined time.

Chemical analysis

400 μL methanol containing 80 ppb M8PFOS and M8PFOA were added to the each 400 μL aliquot, and then filtered through a 0.22 μm nylon. All samples were kept below 4˚C and analyzed within 28 days of experiments. An ultra-performance liquid chromatography coupled with a triple-stage quadrupole mass spectrometer (ACQUITY UPLC-MS/MS, Xevo TQD, Waters Corp., USA) was used for PFAS separation and quantification. The gradient program of UPLC is listed in S1 Table in S1 File. The detailed MS parameters were summarized in S2 Text in S1 File. The standard of quality assurance and quality control was also included in S2 Text in S1 File. The MS transition and detection limit of PFOA/ PFOS are listed in S2 Table in S1 File. M8PFOA and M8PFOS were used as the isotope-label internal standard of PFOA and PFOS, respectively (S3 Table in S1 File).

Results and discussion

Anode characterization

The main crystalline phase of anode was identified by XRD via matching characteristic peak of standard materials (Fig 1A). The XRD patterns of the Ti_4O_7 anode exhibits that it is composed of 74.4% Ti_4O_7, 18.7% Ti_5O_9 and 6.90% Ti_6O_{11}. The SEM result reflects that the Ti_4O_7 anode has a highly porous structure (Fig 1B).

The distribution of pore diameter of the Ti_4O_7 anode was shown in Fig 1C and 1D. The porosity was 21.6%, and the average pore diameter at 4 $V \cdot A^{-1}$ was 2.6 μm. The total pore area was 1.29×10^{-5} cm^2. However, since inner surface of porous anode cannot be accessible by electrolyte, the "outer" surface where the redox reaction can take place, also called effective electroactive surface area (EESA) can better depict the actual reaction sites on porous anode [55–57]. Voltametric method was used to measure EESA of Ti_4O_7 anode [58–60] (S3 Text in S1 File) in different supporting electrolyte solutions, and EESA of anode in different reaction solution are

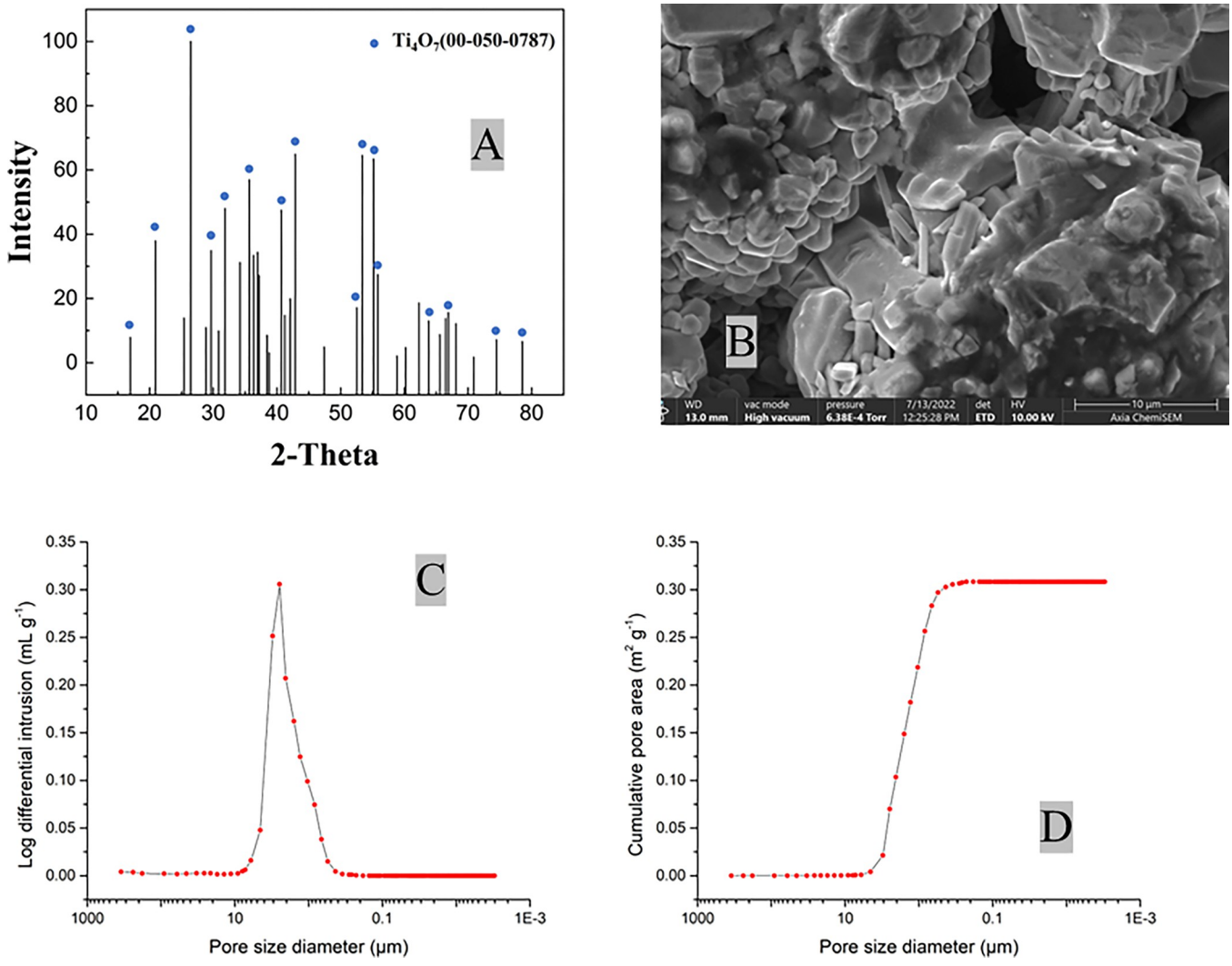

Fig 1. The XRD (A), SEM (B) and mercury intrusion porosimetry analysis on pore size distribution (C) and cumulative pore surface area (D) of the Ti_4O_7 anode. The blue dots represent the characteristic peaks of ICDD Ti4O7 (00-050-0787).

https://doi.org/10.1371/journal.pone.0317696.g001

Table 1. EESA of Ti_4O_7 anodes in different electrolyte solutions.

Electrolyte	EESA (cm^2)
100 mM H_3PO_4	2035.71
100 mM Na_3PO_4	2016 .33
100 mM $NaClO_4$	1927.00
100 mM $NaClO_4$+1 mM $NaNO_3$	1970.66
100 mM $NaClO_4$+5 mM $NaNO_3$	2053.36
100 mM $NaClO_4$+10 mM $NaNO_3$	2356.55
100 mM $NaClO_4$+20 mM $NaNO_3$	2447.65
100 mM $NaClO_4$+1 mM Na_2SO_4	1993.34
100 mM $NaClO_4$+5 mM Na_2SO_4	2110.56
100 mM $NaClO_4$+10 mM Na_2SO_4	2287.86
100 mM $NaClO_4$+20 mM Na_2SO_4	2395.38
100 mM $NaClO_4$+1 mM Na_3PO_4	2264.62
100 mM $NaClO_4$+5 mM Na_3PO_4	2484.64
100 mM $NaClO_4$+10 mM Na_3PO_4	2636.31
100 mM $NaClO_4$+20 mM Na_3PO_4	2730.26
100 mM $NaClO_4$+1 mM Na_2CO_3	1942.86
100 mM $NaClO_4$+5 mM Na_2CO_3	2221.25
100 mM $NaClO_4$+10 mM Na_2CO_3	2238.04
100 mM $NaClO_4$+20 mM Na_2CO_3	2427.57

https://doi.org/10.1371/journal.pone.0317696.t001

presented in Table 1, S4 Table and S1 Fig in S1 File. It appears that adding anions with increasing concentrations help to enhance EESA. This may be because higher electrolyte concentration compresses the diffusion layer at a charged interface, while a thinner diffusion layer results in a higher electroactive surface area [61]. Higher charge valences of different anions may also contribute to thinner diffusion layer [62].

The LSV results of Ti_4O_7 anode in 100 mM $NaClO_4$ solution with different concentration of different anions (1–20 mM) was shown in Fig 2. For NO_3^-, SO_4^{2-} and PO_4^{3-}, the anodic current in reaction solution with only 100 mM $NaClO_4$ was higher than that with other anions added, (Fig 2A, 2B and 2D). It suggests that electrolysis of water was hindered due to reactive sites of Ti_4O_7 anode has been taken up by these anions, leading to reduced generation of $HO^{\cdot}$ on the anode surface [45, 63]. Anode is positively charged, and thus strongly attracts anions, which may block sites for water oxidation to produce hydroxyl free radicals. However, the anodic potential increased with increasing concentration CO_3^{2-} (Fig 2C). It suggests that CO_3^{2-} can be oxidized at lower anodic potential than water [45].

The effect of pH

An EO treatment experiment was conducted with 100 mM H_3PO_4 and 100 mM Na_3PO_4 as the supporting electrolyte solutions, which pH was 1.32 and 12.32, respectively. In The concentration change of PFOA/PFOS are shown in Fig 3. It is seen that PFOA degradation was inhibited when pH was low, while PFOS degradation was not affected by pH change from the acidic to the basic condition. The mass transfer rate of PFOA and PFOS was measured via limiting current method, with 4.20×10^{-5} $m\cdot s^{-1}$ and 4.09×10^{-5} $m\cdot s^{-1}$ obtained, respectively (S4 Text in S1 File), confirming that all the reactions studied in this work were kinetically controlled. In our previous studies, short-chain perfluoroalkyl acids (PFAAs) were observed as the intermediates of PFOA/PFOS degradation during EO tretament by titanium suboxide anodes and near

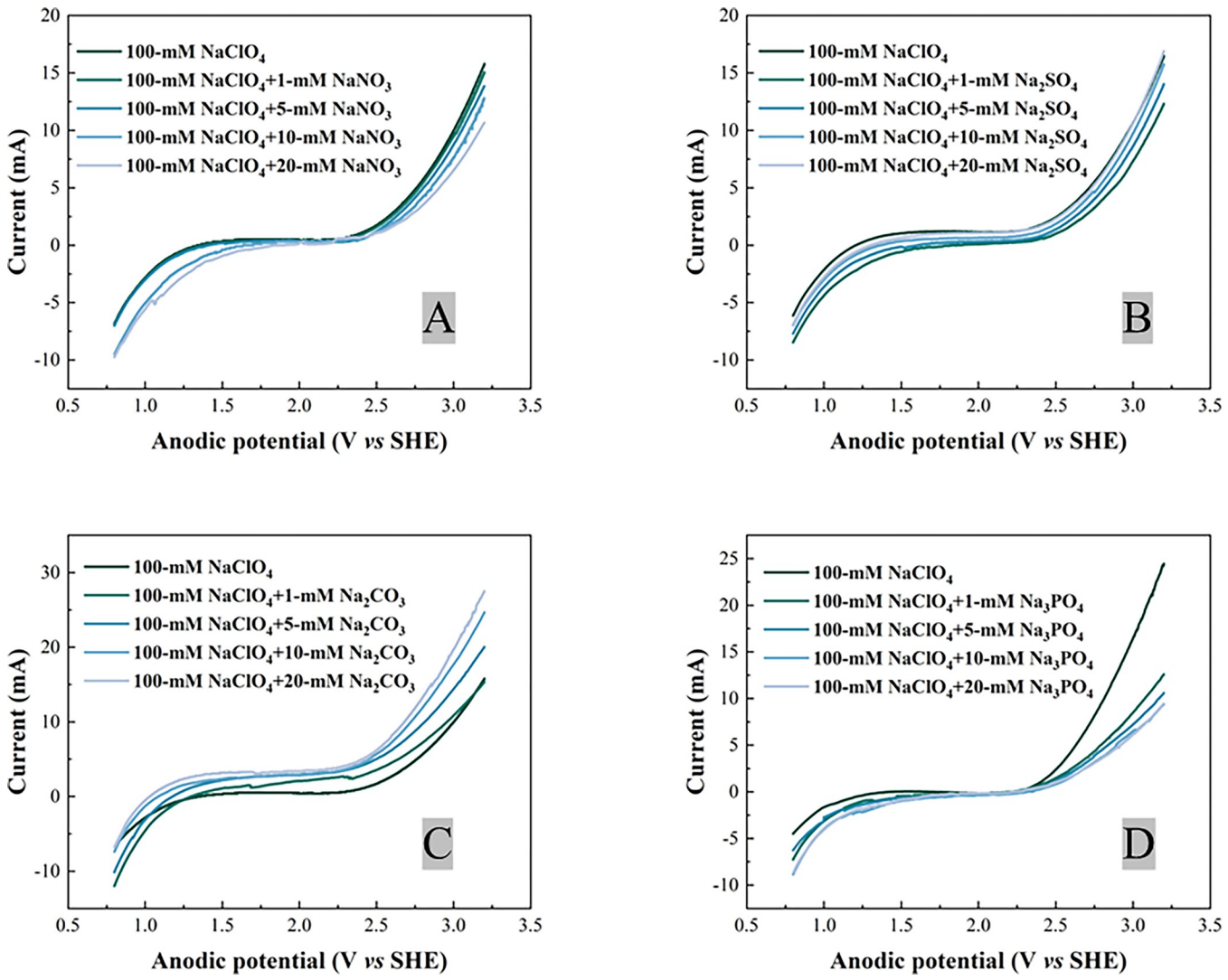

Fig 2. LSV results of the Ti_4O_7 anode in different electrolyte solutions at scan rate 50 $mV \cdot s^{-1}$: NO_3^- (A), SO_42^- (B), CO_3^{2-}(C) and PO_4^{3-} (D).

https://doi.org/10.1371/journal.pone.0317696.g002

complete F^- recovery was achieved [45, 64, 65]. The observed reaction rate constants $k_{obs,PFAS}$ for PFOA/PFOS were calculated via fitting the pseudo-first order reaction model in all system, and the surface area normalized rate constant $k_{SA,PFAS}$ can be calculated by $k_{obs,PFAS}$ normalized to EESA (S5 Text in S1 File). The $k_{SA,PFAS}$ for PFOA degradation was $2.96\times10^{-7}\pm4.24\times10^{-9}$ $m \cdot s^{-1}$ in 100 mM H_3PO_4 solution (pH = 1.32), about 22% lower than that in 100 mM Na_3PO_4 solution (pH = 12.32), which was $3.61\times10^{-7}\pm2.45\times10^{-8}$ $m \cdot s^{-1}$. It is likely that a larger fraction of the anionic form of PFOA because of deprotonation at higher pH facilitates mass transfer towards positively charged anode and oxidation. Furthermore, the $k_{SA,PFAS}$ of PFOS degradation were $3.98\times10^{-7}\pm1.85\times10^{-8}$ $m \cdot s^{-1}$ in 100 mM H_3PO_4 solution (pH = 1.32), similar to that in 100 mM Na_3PO_4 solution (pH = 12.32), which is $4.01\times10^{-7}\pm3.79\times10^{-8}$ $m \cdot s^{-1}$. The pKa of PFOS is around -3.27 [66], and the dominant form is PFOS anion in the reaction solutions with pH at 1.32 or 12.32. Therefore, the degradation of PFOS was not affected at the pH values studied herein.

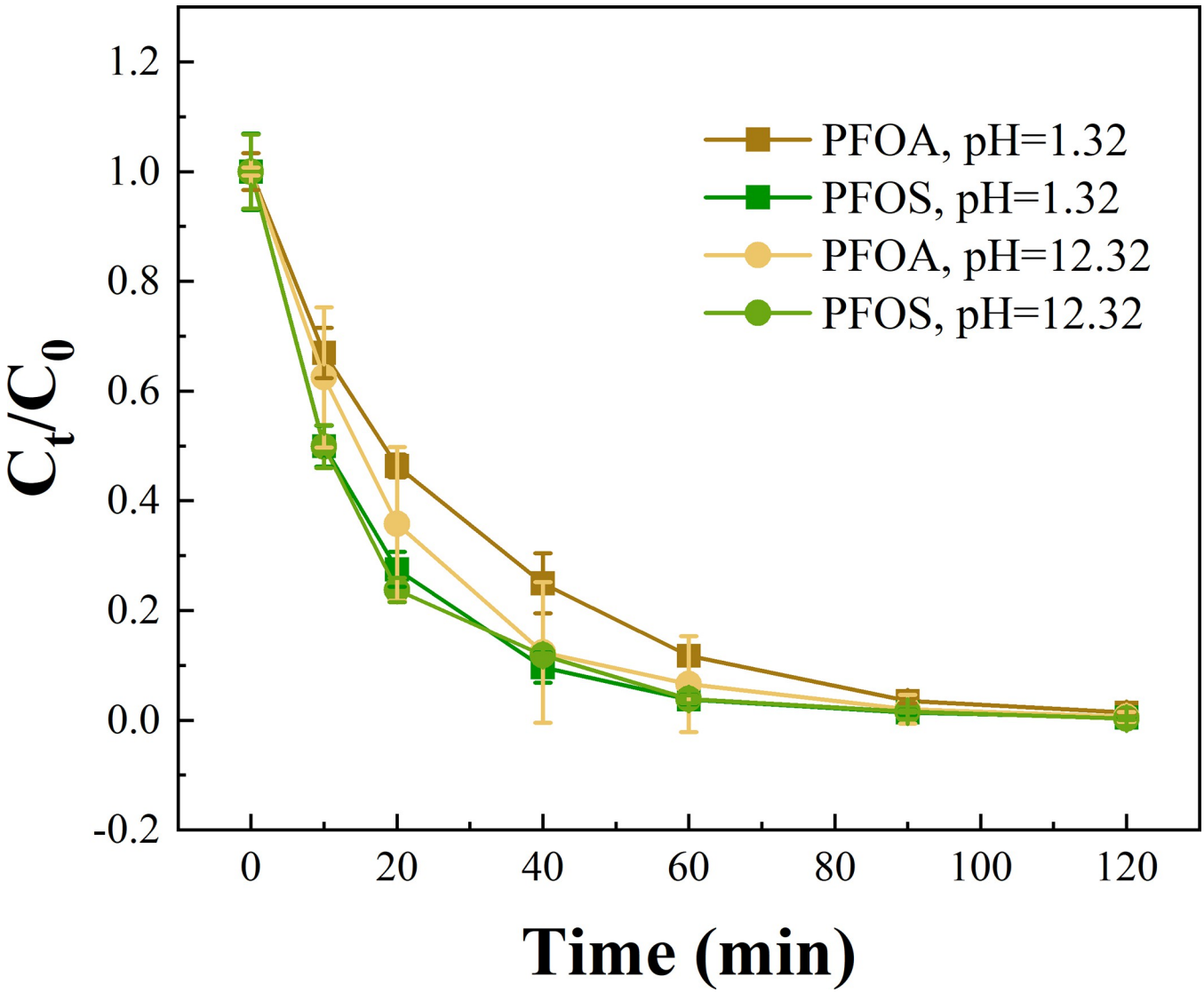

Fig 3. Concentration changes of PFOA/PFOS during EO on the Ti_4O_7 anodes at 10 mA·cm^{-2} in 100 mM H_3PO_4 (pH = 1.32) and 100 mM Na_3PO_4 (pH = 12.32).

https://doi.org/10.1371/journal.pone.0317696.g003

The effect of nitrate ion

The concentration profile of PFOA and PFOS during EO on the Ti_4O_7 anodes at current density 10 mA·cm^{-2} in 100 mM $NaClO_4$ with varying concentrations of $NaNO_3$ are presented in S2 Fig in S1 File. The addition of different anions, including NO_3^-, at different concentrations slightly increased the reaction solution conductivity (S3A Fig in S1 File), for example, the conductivity of 100 mM $NaClO_4$ solution was 10.36 mS·cm^{-1}, and it rose to 12.07 mS·cm^{-1} when 20 mM NO_3^- was added into the system. However, the AP slightly decreased with different anions added at different concentrations (S3B Fig in S1 File). As shown in S2A Fig in S1 File, after 60 min EO treatment, 80.2% PFOA was removed from the reaction solution with 100 mM $NaClO_4$ as the only electrolyte, while 83.4% and 86.6% PFOA was degraded when 5.0 mM and 1.0 mM $NaNO_3$ was added, respectively, indicating promoted degradation of PFOA. However, such promotion effect was reversed with further increase of NO_3^- concentration.

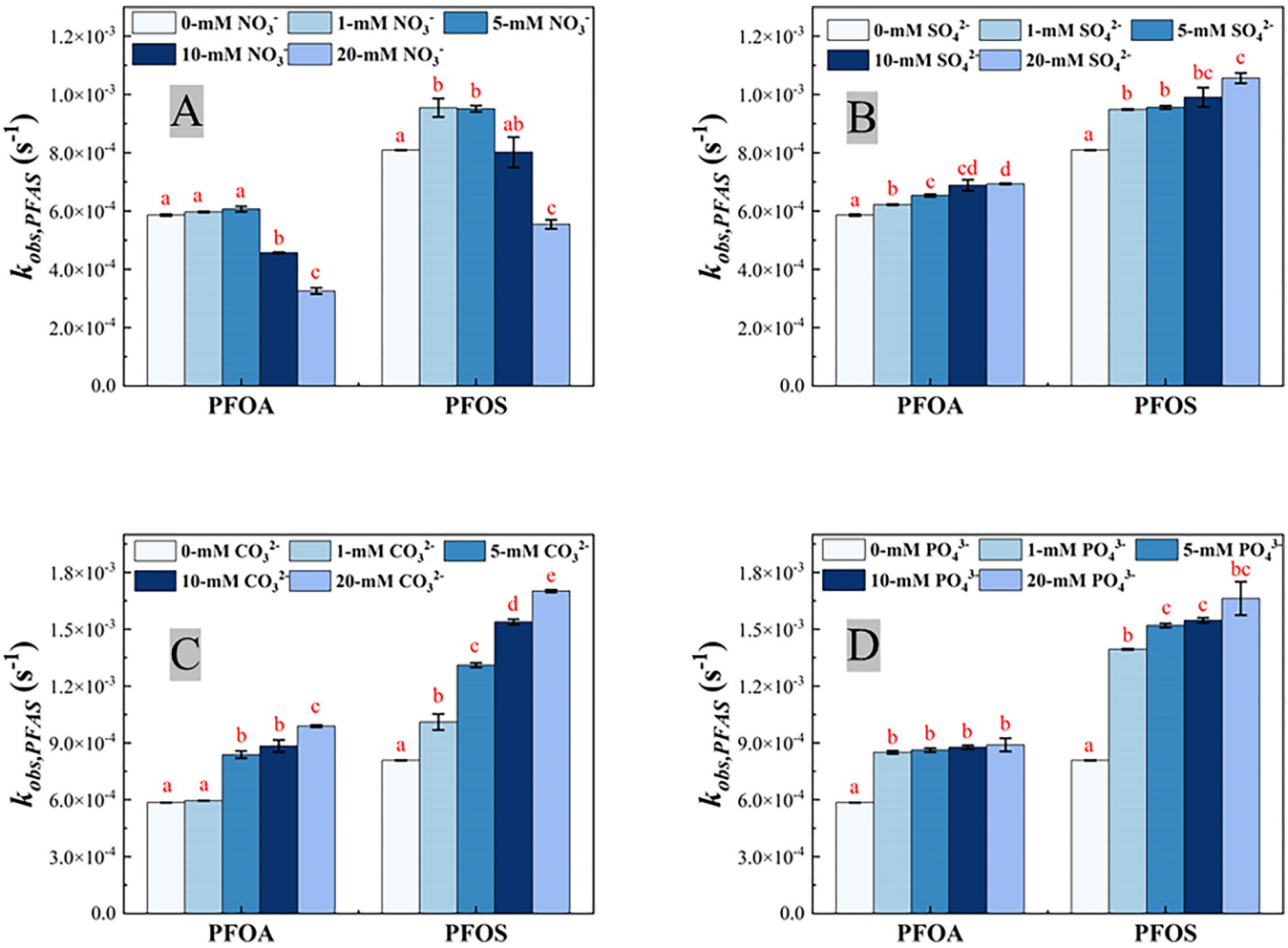

Fig 4. Observed reaction rate constant $k_{obs,PFAS}$ for PFOA and PFOS degradation on the Ti_4O_7 anode in 100 mM $NaClO_4$ with different concentrations of NO_3^- (A), SO_4^{2-} (B), CO_3^{2-}(C) and PO_4^{3-} (D). The same letter indicates no statistical difference at $\alpha = 0.05$, for the comparison of the $k_{obs,PFAS}$ of PFOA/PFOS degradation of the same anions with different concentrations. Initial PFOA/PFOS concentration: 2 μM. Error bar represents standard deviations of replicates.

https://doi.org/10.1371/journal.pone.0317696.g004

The degradation of PFOA after 60 min was decreased to 69.0% and 61.2% when NO_3^- concentration increased to 10 mM and 20 mM, respectively (S2A Fig in S1 File). PFOS degradation was faster than PFOA in the same reaction condition and exhibited a similar trend with PFOA. 93.7% PFOS was degraded on Ti_4O_7 anode after 60 mins without NO_3^- added. The removal ratio increased to 98.1% and 97.8% when 1 mM and 5 mM $NaNO_3$ were added to the reaction solution, respectively. However, when NO_3^- concentration increased to 10 mM and 20 mM, the removal ratio decreased to 93.1% and 75.6%, respectively. The k_{obs} and k_{SA} values at varying NO_3^- concentrations are reported in Figs 4 and 5, respectively, as well as SO_4^{2-}, PO_4^{3-} and CO_3^{2-}, with results of ANOVA tests (S6 Text in S1 File) indicated. The k_{obs} and the k_{SA} for PFOA and PFOS in different electrolyte solutions are also summarized in S5 Table in S1 File.

As shown in Fig 4A, although the reaction rate constant ($k_{obs,PFAS}$) did not vary much when 1 mM or 5 mM NO_3^- added, there was a marked drop in $k_{obs,PFAS}$ when NO_3^- concentration increased to 10 mM and 20 mM. The $k_{obs,PFAS}$ of PFOA decreasing from $6.07\times10^{-4}\pm9.43\times10^{-6}$ s^{-1} to $3.26\times10^{-4}\pm1.06\times10^{-5}$ s^{-1} when NO_3^- concentration increased from 5 mM to 20 mM.

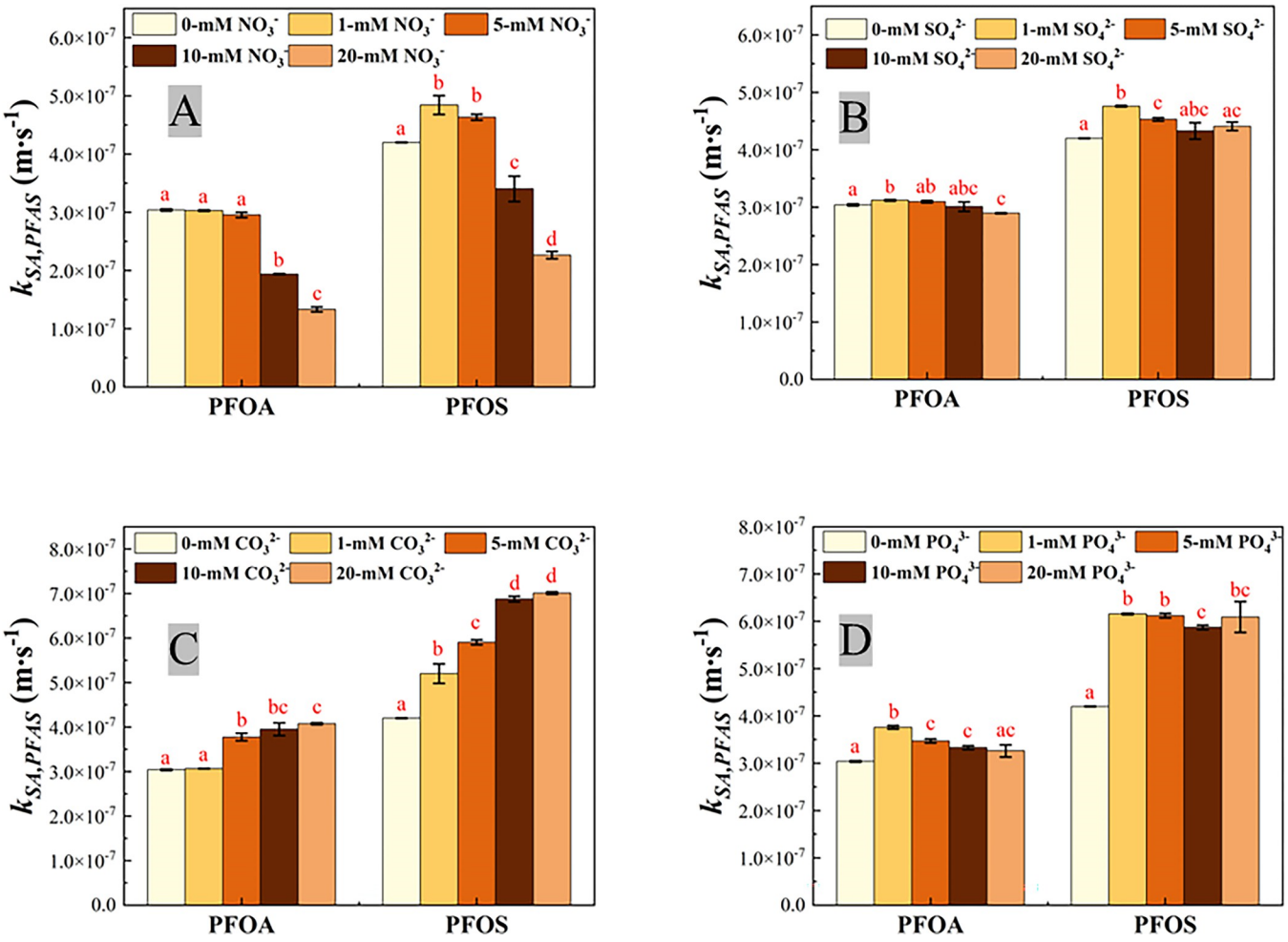

Fig 5. Surface area normalized reaction rate constant $k_{SA,PFAS}$ for PFOA and PFOS degradation on the Ti_4O_7 anode in 100 mM $NaClO_4$ with different concentrations of NO_3^- (A), SO_42^- (B), CO_3^{2-}(C) and PO_4^{3-} (D). The same letter indicates no statistical difference at $\alpha = 0.05$, for the comparison of the $k_{SAs,PFAS}$ of PFOA/PFOS degradation of the same anions with different concentrations. Initial PFOA/PFOS concentration: 2 μM. Error bar represents standard deviations of replicates.

https://doi.org/10.1371/journal.pone.0317696.g005

Moreover, it is evident in Fig 5A that the surface area normalized rate constant $k_{SA,PFAS}$ decreased along with increasing NO_3^- in the background solution, indicating that PFOA/PFOS degradation was hindered in the presence of NO_3^- with concentration higher than 10 mM. Such inhibition effect can be explained by the LSV results (Fig 2A). The anodic current decreased with increasing NO_3^- concentration. It may suggest that NO_3^- occupied the reactive sites on anode surface and hindered the electrolysis of water, which can be further confirmed by the quenching experiment using p-chlorobenzoic acid (pCBA) as the hydroxyl radical scavenger (see S7 Text in S1 File for detail). The steady-state hydroxyl radical concentration ($[HO^{\cdot}]_{ss}$) can be calculated via Equation S-7 in SI. Note that the EESA increased with increasing concentration of anions in the reaction solution (S1 Fig in S1 File). The $[HO^{\cdot}]_{ss}$ and EESA-normalized $[HO^{\cdot}]_{ss}$ are listed in S6 Table in S1 File. The EESA-normalized $[HO^{\cdot}]_{ss}$ was 1.20×10^{-17} M·cm^{-2} in 100 mM $NaClO_4$ solution, and it reduced to 1.19×10^{-17}, 1.14×10^{-17}, 6.66×10^{-18} and 6.02×10^{-18} M·cm^{-2} when 1 mM, 5 mM, 10 mM and 20 mM NO_3^- was added, respectively. Furthermore, nitrate ion can react with $HO^{\cdot}$ to form nitrate radicals via reaction (1) that further consume$HO^{\cdot}$ in EO system, however, nitrate radicals do not have high

reactivity to degrade PFOA and PFOS [67, 68]. Because $HO^{\cdot}$ is essential to PFOA/PFOS degradation [41, 45], the presence of NO_3^- led to inhibited degradation of PFOA/PFOS (Fig 5A) by reducing EESA-normalized steady-state concentration of $HO^{\cdot}$ (S6 Table in S1 File).

$$HO^{\cdot} + NO_3^- \rightarrow HO^- + NO_3^{\cdot} \quad (1)$$

The effect of sulfate ion

The degradation curve of PFOA and PFOS on the Ti_4O_7 anode at 10 $mA{\cdot}cm^{-2}$ in 100 mM $NaClO_4$ solution with varying concentrations of Na_2SO_4 are exhibited in S4 Fig in S1 File. PFOA/PFOS degradation increased slightly along with increasing concentration of SO_4^{2-} added in the background. After 60 min EO treatment, 80.2% PFOA were removed with 100 mM $NaClO_4$ as the only electrolyte, while 85.3%, 87.4%, 88.7% and 89.8% PFOA was degraded when 1.0 mM, 5.0 mM, 10 mM and 20 mM Na_2SO_4 was added, respectively (S4A Fig in S1 File). PFOS degradation showed a similar trend (S4B Fig in S1 File). The observed reaction rate constant $k_{obs,PFAS}$ increased from $5.86\times10^{-4}\pm3.54\times10^{-6}$ s^{-1} for PFOA and $8.09\times10^{-4}\pm1.18\times10^{-6}$ s^{-1} for PFOS in the absence of SO_4^{2-} to $6.93\times10^{-4}\pm2.36\times10^{-6}$ s^{-1} for PFOA and $1.06\times10^{-3}\pm1.77\times10^{-5}$ s^{-1} for PFOS in the presence of 20 mM SO_4^{2-}, respectively (Fig 4B, S5 Table in S1 File). However, the change of surface area normalized rate constant $k_{SA,PFAS}$ of PFOA was nearly negligible, while the $k_{SA,PFAS}$ of PFOS was slightly decreased when SO_4^{2-} concentration was above 1mM, $3.04\times10^{-7}\pm1.83\times10^{-9}$ $m{\cdot}s^{-1}$ for PFOA and $4.20\times10^{-7}\pm6.12\times10^{-10}$ $m{\cdot}s^{-1}$ for PFOS in the absence of SO_4^{2-} versus $2.89\times10^{-7}\pm9.84\times10^{-10}$ $m{\cdot}s^{-1}$ for PFOA and $4.41\times10^{-7}\pm7.38\times10^{-8}$ $m{\cdot}s^{-1}$ for PFOS in the presence of 20 mM SO_4^{2-}, respectively (Fig 5B, S5 Table in S1 File). The $[HO^{\cdot}]_{ss}$ was also quantified. The pCBA degradation slightly accelerated when higher concentration of SO_4^{2-} was added (S5 Fig in S1 File), but EESA-normalized $[HO^{\cdot}]_{ss}$ remain at the same level (S7 Table in S1 File). It indicates that higher SO_4^{2-} concentration promoted $HO^{\cdot}$ formation, mainly because greater effective electroactive surface area (Table 1) became available for $HO^{\cdot}$ formation, and thus facilitated PFOA/PFOS degradation.

The effect of carbonate ion

S6 Fig in S1 File shows the concentration profile of PFOA/PFOS during 120 min EO treatment in 100-mM $NaClO_4$ with different concentrations of Na_2CO_3. When current applied, the pH of reaction solution quickly increased and stabilized at 10.7–12.1 (S7 Fig in S1 File). Because the pKa_1 and pKa2 of H_2CO_3 are 6.35 and 10.33, respectively [69], CO_3^{2-} was the main form in the reaction solution rather than HCO_3^-. As shown in S6A Fig in S1 File, the PFOA/PFOS degradation was speeded up in the presence of CO_3^{2-}, with 81.1%, 94.6%, 95.2% and 96.8% PFOA removal achieved respectively with 1 mM, 5 mM, 10 mM and 20 mM CO_3^{2-} in the reaction solution, compared to 80.2% PFOA removal in the absence of CO_3^{2-} after 60 min EO treatment on the Ti_4O_7 anode. PFOS degradation exhibited a similar trend (S6B Fig in S1 File). Both $k_{obs,PFAS}$ and $k_{SA,PFAS}$ values are increased with increasing CO_3^{2-} concentration in the background solution (Figs 4C and 5C), indicating that the presence of CO_3^{2-} enhanced the degradation of PFOA/PFOS. The $k_{obs,PFOA}$ were $5.96\times10^{-4}\pm1.18\times10^{-6}$ s^{-1}, $8.38\times10^{-4}\pm1.89\times10^{-5}$ s^{-1}, $8.84\times10^{-4}\pm3.18\times10^{-5}$ s^{-1}, $9.89\times10^{-4}\pm5.89\times10^{-6}$ s^{-1} with 1 mM, 5 mM, 10 mM and 20 mM CO_3^{2-} added, respectively, compared to $5.86\times10^{-4}\pm3.54\times10^{-6}$ s^{-1} without Na_2CO_3 salt added. Likewise, the $k_{SA,PFOA}$ increased from $3.04\times10^{-7}\pm1.83\times10^{-9}$ $m{\cdot}s^{-1}$ in the absence Na_2CO_3 salt to $3.07\times10^{-7}\pm6.07\times10^{-10}$ $m{\cdot}s^{-1}$, $3.77\times10^{-7}\pm8.49\times10^{-9}$ $m{\cdot}s^{-1}$, $3.95\times10^{-7}\pm1.42\times10^{-8}$ $m{\cdot}s^{-1}$, and $4.07\times10^{-7}\pm2.43\times10^{-9}$ $m{\cdot}s^{-1}$ with 1 mM, 5 mM, 10 mM and 20 mM CO_3^{2-} added, respectively. However, pCBA degradation cannot be detected when the concentration of CO_3^{2-} was higher than 5 mM (S8 Fig in S1 File), indicating that CO_3^{2-} can scavenge $HO^{\cdot}$ generated in the EO system. CO_3^{2-} can react with $HO^{\cdot}$ to produce carbonate radical anion ($CO_3^{\cdot-}$) by one-electron

transfer between carbonate ion and hydroxyl free radical ($HO^{\cdot}$) via reaction (2) [70]. CO_3^{2-} can also be oxidized to $CO_3^{\cdot-}$ via losing one electron via reaction (3) [71], which can be evidenced by LSV result (Fig 2D). $CO_3^{\cdot-}$ is a strong oxidizing agent [72]. Compared to $HO^{\cdot}$, $CO_3^{\cdot-}$ is more selective, targeting on the persistent organic pollutants, especially those that are electron-rich [73]. $CO_3^{\cdot-}$ was proved to have the capability of promoting the degradation of PFOA, especially in alkaline solution in both photochemical decomposition and sonochemical treatment [73–75]. If and how $CO_3^{\cdot-}$ may facilitates PFAS degradation during EO needs more exploration.

$$HO^{\cdot} + CO_3^{2-} \rightarrow HO^{-} + CO_3^{\cdot-} (k = 3.0 \times 10^8\ M^{-1} \cdot s^{-1}) \quad (2)$$

$$CO_3^{2-} \rightarrow CO_3^{\cdot-} + e_{aq}^{-} \quad (3)$$

The effect of phosphate ion

S9 Fig in S1 File shows the PFOA/PFOS concentration profiles during 120 min EO treatment in 100 mM $NaClO_4$ with different concentrations of Na_3PO_4. Like CO_3^{2-}, increasing PO_4^{3-} concentration promoted PFOA/PFOS degradation. After 60 min EO treatment, 80.2% PFOA was removed in 100 mM $NaClO_4$ solution, while 94.6%, 94.8%, 96.0% and 96.9% PFOA was degraded when 1.0 mM, 5.0 mM, 10 mM and 20 mM Na_3PO_4 was added, respectively (S9A Fig in S1 File). PFOS degradation exhibited a similar trend (S9B Fig in S1 File). For PFOA degradation, the change of $k_{obs,PFOA}$ was negligible with increasing Na_3PO_4 salt added, from $8.51\times10^{-4}\pm8.25\times10^{-6}$ s^{-1} with 1 mM Na_3PO_4 added to $8.90\times10^{-4}\pm3.54\times10^{-5}$ s^{-1} with 20 mM Na_3PO_4 added (Fig 4D), while $k_{SA,PFOA}$ slightly decreased with increasing Na_3PO_4 salt added, from $3.76\times10^{-7}\pm3.64\times10^{-9}$ $m\cdot s^{-1}$ with 1 mM Na_3PO_4 added to $3.26\times10^{-7}\pm1.29\times10^{-8}$ s^{-1} with 20 mM Na_3PO_4 added (Fig 5D). However, for PFOS degradation, the $k_{obs,PFOS}$ slightly increased with increasing Na_3PO_4 salt added, from $1.39\times10^{-3}\pm3.54\times10^{-6}$ s^{-1} with 1 mM Na_3PO_4 added to $1.66\times10^{-3}\pm8.84\times10^{-5}$ s^{-1} with 20 mM Na_3PO_4 added (Fig 4D), while the change of $k_{SA,PFOS}$ was negligible with increasing Na_3PO_4 salt added, from $6.16\times10^{-7}\pm1.56\times10^{-9}$ $m\cdot s^{-1}$ with 1 mM Na_3PO_4 added to $6.09\times10^{-7}\pm3.24\times10^{-8}$ s^{-1} with 20 mM Na_3PO_4 added (Fig 5D). The pH change during EO treatment was shown in S10 Fig in S1 File. The pKa1, pKa2 and pKa3 of phosphoric acid are 2.15, 7.20 and 12.4, respectively [69]. When Na_3PO_4 concentrations increased from 1 mM to 20 mM, the pH increased from 12.04 to 12.46 at the end of 2 h experiment (S10 Fig in S1 File), and thus the dominant form changed from hydrogen phosphate ions (HPO_4^{2-}) to phosphate ions (PO_4^{3-}). HPO_4^{2-} and PO_4^{3-} can react with $HO^{\cdot}$ to form hydrogen phosphate radicals and phosphate radicals via reaction (4) and (5), respectively. It is further evidenced by delayed pCBA degradation (S11 Fig in S1 File). Delayed pCBA degradation indicates that $HO^{\cdot}$ was scavenged by HPO_4^{2-} and PO_4^{3-} in EO system [67, 76]. Phosphate radicals are selective oxidants whose reactivity are comparable with $HO^{\cdot}$, which are capable of promoting organic compounds degradation via one-electron oxidation [67, 77, 78], as well as that of PFOA/PFOS during EO as shown in Fig 4D. Phosphate radicals may reacts preferentially with PFOS, leading to slight increase $k_{obs,PFOS}$ (Fig 4D), but still needs further verification. However, when PO_4^{3-} concentration increased further, excessive PO_4^{3-} can couple with another PO_4^{3-} to form peroxodiphosphate with two electrons extracted in alkaline solution via reaction (6) [79–81]. Peroxodiphosphate behaves as a soft oxidant in the oxidation of organics [82], which may not have the capability to attack PFOA/PFOS molecules. It is known that radical-mediated reactions play an important role in PFOA/PFOS degradation [41, 64]. Therefore, PFOA/PFOS degradation was accelerated (Fig 4D) due to larger EESA of Ti_4O_7 anode (Table 1) and strong oxidant formation of phosphate radicals when PO_4^{3-} was added, but further increasing PO_4^{3-} concentration led to more and more $P_2O_8^{4-}$ formed on the anode

surface, suppressing the formation of phosphate radicals, so that the EESA-normalized reaction rate constant of PFOA/PFOS tended to decrease with increasing PO_4^{3-} (Fig 5D).

$$HPO_4^{2-} + HO^{\cdot} \rightarrow HPO_4^{\cdot-} + HO^{-} \quad (4)$$

$$PO_4^{3-} + HO^{\cdot} \rightarrow PO_4^{2-\cdot} + HO^{-} \quad (5)$$

$$PO_4^{3-} + PO_4^{3-} \rightarrow P_2O_8^{4-} + 2e^{-} \quad (6)$$

Overall, SO_4^{2-}, CO_3^{2-} and PO_4^{3-} promoted PFOA/PFOS degradation, while NO_3^{-} hindered it, when its concentration was higher than 10 mM (Fig 4A). Such inhibition effect of NO_3^{-} resulted from reduced EESA-normalized steady-state concentration of $HO^{\cdot}$ (S6 Table in S1 File), which plays an vital role in PFOA/PFOS degradation [41]. The presence of SO_4^{2-} accelerated PFOA/PFOS degradation due to higher $HO^{\cdot}$ formation caused by enlarged EESA. CO_3^{2-} reacted with $HO^{\cdot}$ to form a strong and selective oxidant, $CO_3^{\cdot-}$, that has the capability of promoting PFOA/PFOS degradation by one-electron transfer reaction. Phosphate radicals, formed by the reaction between PO_4^{3-}/HPO_4^{2-} and $HO^{\cdot}$, was also able to promote PFOA/PFOS degradation, but peroxodiphosphate ion was generated and suppressed the formation of phosphate radicals, when PO_4^{3-} was beyond 1 mM (Fig 5D), leading to delayed PFOA/PFOS degradation.

Conclusions

The EO treatment of PFOA and PFOS, two representative PFASs, were conducted in reaction solutions with varying concentrations of different anions, including NO_3^{-}, SO_4^{2-}, CO_3^{2-} and PO_4^{3-}. The acidity of the solution delayed PFOA degradation in relation to its acid dissociation behavior, but did not affect the PFOS degradation at the tested pH 1.32 and 12.32. NO_3^{-} significantly hindered PFOA/PFOS degradation due to suppressed $HO^{\cdot}$ generation, which plays an important role in PFAS degradation. PO_4^{3-} slightly promoted PFOA/PFOS degradation, but phosphate radicals formation were suppressed by forming $P_2O_8^{4-}$ simultaneously, delaying PFOA/PFOS degradation at high PO_4^{3-} concentration. Increasing concentration of SO_4^{2-} helped to increase EESA, and thus the observed degradation rates of PFOA/PFOS during EO, because more surface on the anode became accessible for EO reactions. The presence of CO_3^{2-} greatly enhanced the degradation of PFOA/PFOS on account of the generation of $CO_3^{\cdot-}$, which can directly oxidize the perfluorinated carboxyl anions to form highly reactive radicals, and thus promoting the subsequent -CF_2- unzipping processes. The information obtained in this study can help guide the implementation of Ti_4O_7-based EO treatment for PFAS removal in waters, particularly in industrial and municipal wastewater where large amounts of anions are present.

Supporting information

S1 File.
(PDF)

Acknowledgments

I would like to extend my sincere gratitude to the funding agencies and organizations that have provided financial support for this research. I am also grateful for the dedication, commitment, and professionalism demonstrated by each team member.

Author Contributions

Conceptualization: Yaye Wang, Qingguo Huang.

Data curation: Yaye Wang, Yifei Wang, Shuping Dong.

Formal analysis: Yaye Wang.

Funding acquisition: Qingguo Huang.

Investigation: Yaye Wang, Qingguo Huang.

Methodology: Yaye Wang, Qingguo Huang.

Project administration: Qingguo Huang.

Resources: Qingguo Huang.

Software: Yaye Wang.

Validation: Yaye Wang.

Visualization: Yaye Wang.

Writing – original draft: Yaye Wang.

Writing – review & editing: Yaye Wang, Yifei Wang, Shuping Dong, Qingguo Huang.

References

1. Ritscher A, Wang Z, Scheringer M, Boucher JM, Ahrens L, Berger U, et al. Zürich statement on future actions on per-and polyfluoroalkyl substances (PFASs). Environmental health perspectives. 2018; 126 (8):084502.
2. Buck RC, Franklin J, Berger U, Conder JM, Cousins IT, De Voogt P, et al. Perfluoroalkyl and polyfluoroalkyl substances in the environment: terminology, classification, and origins. Integrated environmental assessment and management. 2011; 7(4):513–41. https://doi.org/10.1002/ieam.258 PMID: 21793199
3. Ahrens L, Shoeib M, Harner T, Lee SC, Guo R, Reiner EJ. Wastewater Treatment Plant and Landfills as Sources of Polyfluoroalkyl Compounds to the Atmosphere. Environmental Science & Technology. 2011; 45(19):8098–105. https://doi.org/10.1021/es1036173 PMID: 21466185
4. Brusseau ML, Anderson RH, Guo B. PFAS concentrations in soils: Background levels versus contaminated sites. Science of The Total Environment. 2020; 740:140017. https://doi.org/10.1016/j.scitotenv.2020.140017 PMID: 32927568
5. Høisæter Å, Pfaff A, Breedveld GD. Leaching and transport of PFAS from aqueous film-forming foam (AFFF) in the unsaturated soil at a firefighting training facility under cold climatic conditions. Journal of Contaminant Hydrology. 2019; 222:112–22. https://doi.org/10.1016/j.jconhyd.2019.02.010 PMID: 30878240
6. Huset CA, M. Barry K. Quantitative determination of perfluoroalkyl substances (PFAS) in soil, water, and home garden produce. MethodsX. 2018; 5:697–704. https://doi.org/10.1016/j.mex.2018.06.017 PMID: 29998069
7. Rankin K, Mabury SA, Jenkins TM, Washington JW. A North American and global survey of perfluoroalkyl substances in surface soils: Distribution patterns and mode of occurrence. Chemosphere. 2016; 161:333–41. https://doi.org/10.1016/j.chemosphere.2016.06.109.
8. Cheng J, Vecitis CD, Park H, Mader BT, Hoffmann MR. Sonochemical Degradation of Perfluorooctane Sulfonate (PFOS) and Perfluorooctanoate (PFOA) in Groundwater: Kinetic Effects of Matrix Inorganics. Environmental Science & Technology. 2010; 44(1):445–50. https://doi.org/10.1021/es902651g PMID: 19950930
9. Moody CA, Hebert GN, Strauss SH, Field JA. Occurrence and persistence of perfluorooctanesulfonate and other perfluorinated surfactants in groundwater at a fire-training area at Wurtsmith Air Force Base, Michigan, USA. Journal of Environmental Monitoring. 2003; 5(2):341–5. https://doi.org/10.1039/b212497a PMID: 12729279
10. Xiao F, Simcik MF, Halbach TR, Gulliver JS. Perfluorooctane sulfonate (PFOS) and perfluorooctanoate (PFOA) in soils and groundwater of a U.S. metropolitan area: Migration and implications for human exposure. Water Research. 2015; 72:64–74. https://doi.org/10.1016/j.watres.2014.09.052 PMID: 25455741

11. Guelfo JL, Adamson DT. Evaluation of a national data set for insights into sources, composition, and concentrations of per- and polyfluoroalkyl substances (PFASs) in U.S. drinking water. Environmental Pollution. 2018; 236:505–13. https://doi.org/10.1016/j.envpol.2018.01.066 PMID: 29427949

12. Sharma BM, Bharat GK, Tayal S, Larssen T, Bečanová J, Karásková P, et al. Perfluoroalkyl substances (PFAS) in river and ground/drinking water of the Ganges River basin: Emissions and implications for human exposure. Environmental Pollution. 2016; 208:704–13. https://doi.org/10.1016/j.envpol.2015.10.050 PMID: 26561452

13. Wang Z, DeWitt JC, Higgins CP, Cousins IT. A Never-Ending Story of Per- and Polyfluoroalkyl Substances (PFASs)? Environmental Science & Technology. 2017; 51(5):2508–18. https://doi.org/10.1021/acs.est.6b04806 PMID: 28224793

14. Gilliland FD, Mandel JS. Serum perfluorooctanoic acid and hepatic enzymes, lipoproteins, and cholesterol: A study of occupationally exposed men. American Journal of Industrial Medicine. 1996; 29 (5):560–8. https://doi.org/10.1002/(SICI)1097-0274(199605)29:5<560::AID-AJIM17>3.0.CO;2-Z. PMID: 8732932

15. Khalil N, Lee M, Steenland K. Epidemiological Findings. In: DeWitt JC, editor. Toxicological Effects of Perfluoroalkyl and Polyfluoroalkyl Substances. Cham: Springer International Publishing; 2015. p. 305–35.

16. Negri E, Metruccio F, Guercio V, Tosti L, Benfenati E, Bonzi R, et al. Exposure to PFOA and PFOS and fetal growth: a critical merging of toxicological and epidemiological data. Critical Reviews in Toxicology. 2017; 47(6):489–515. https://doi.org/10.1080/10408444.2016.1271972 PMID: 28617200

17. Apelberg BJ, Goldman LR, Calafat AM, Herbstman JB, Kuklenyik Z, Heidler J, et al. Determinants of Fetal Exposure to Polyfluoroalkyl Compounds in Baltimore, Maryland. Environmental Science & Technology. 2007; 41(11):3891–7. https://doi.org/10.1021/es0700911 PMID: 17612165

18. Barry V, Winquist A, Steenland K. Perfluorooctanoic Acid (PFOA) Exposures and Incident Cancers among Adults Living Near a Chemical Plant. Environ Health Perspect. 2013; 121(11–12):1313–8. https://doi.org/10.1289/ehp.1306615 PMID: 24007715

19. Nicole W. PFOA and cancer in a highly exposed community: new findings from the C8 science panel. Environ Health Perspect. 2013; 121(11–12):A340–A. Epub 2013/12/01. https://doi.org/10.1289/ehp.121-A340 PMID: 24284021.

20. USEPA. Per- and Polyfluoroalkyl Substances (PFAS) Final PFAS National Primary Drinking Water Regulation. 2024.

21. Schröder HF, Meesters RJW. Stability of fluorinated surfactants in advanced oxidation processes—A follow up of degradation products using flow injection–mass spectrometry, liquid chromatography–mass spectrometry and liquid chromatography–multiple stage mass spectrometry. Journal of Chromatography A. 2005; 1082(1):110–9. https://doi.org/10.1016/j.chroma.2005.02.070 PMID: 16038200

22. Vecitis CD, Park H, Cheng J, Mader BT, Hoffmann MR. Treatment technologies for aqueous perfluorooctanesulfonate (PFOS) and perfluorooctanoate (PFOA). Frontiers of Environmental Science & Engineering in China. 2009; 3(2):129–51. https://doi.org/10.1007/s11783-009-0022-7

23. Javed H, Lyu C, Sun R, Zhang D, Alvarez PJJ. Discerning the inefficacy of hydroxyl radicals during perfluorooctanoic acid degradation. Chemosphere. 2020; 247:125883. https://doi.org/10.1016/j.chemosphere.2020.125883 PMID: 31978654

24. Hendren Z, Kim GD, Kim J. Effective Destruction of PFAS in Water by Modified SiC-Based Photocatalysts. SERDP Project ER18-1513: October, 2019. Report No.

25. Liu J, Qu R, Wang Z, Mendoza-Sanchez I, Sharma VK. Thermal- and photo-induced degradation of perfluorinated carboxylic acids: Kinetics and mechanism. Water Research. 2017; 126:12–8. https://doi.org/10.1016/j.watres.2017.09.003 PMID: 28917116

26. Cao H, Zhang W, Wang C, Liang Y. Sonochemical degradation of poly- and perfluoroalkyl substances–A review. Ultrasonics Sonochemistry. 2020; 69:105245. https://doi.org/10.1016/j.ultsonch.2020.105245 PMID: 32702636

27. Lewis AJ, Joyce T, Hadaya M, Ebrahimi F, Dragiev I, Giardetti N, et al. Rapid degradation of PFAS in aqueous solutions by reverse vortex flow gliding arc plasma. Environmental Science: Water Research & Technology. 2020; 6(4):1044–57. https://doi.org/10.1039/C9EW01050E

28. Singh RK, Brown E, Mededovic Thagard S, Holsen TM. Treatment of PFAS-containing landfill leachate using an enhanced contact plasma reactor. Journal of Hazardous Materials. 2021; 408:124452. https://doi.org/10.1016/j.jhazmat.2020.124452 PMID: 33243646

29. Hao S, Choi Y-J, Wu B, Higgins CP, Deeb R, Strathmann TJ. Hydrothermal Alkaline Treatment for Destruction of Per- and Polyfluoroalkyl Substances in Aqueous Film-Forming Foam. Environmental Science & Technology. 2021; 55(5):3283–95. https://doi.org/10.1021/acs.est.0c06906 PMID: 33557522

30. Wu B, Hao S, Choi Y, Higgins CP, Deeb R, Strathmann TJ. Rapid Destruction and Defluorination of Perfluorooctanesulfonate by Alkaline Hydrothermal Reaction. Environmental Science & Technology Letters. 2019; 6(10):630–6. https://doi.org/10.1021/acs.estlett.9b00506

31. Wang L, Batchelor B, Pillai SD, Botlaguduru VSV. Electron beam treatment for potable water reuse: Removal of bromate and perfluorooctanoic acid. Chemical Engineering Journal. 2016; 302:58–68. https://doi.org/10.1016/j.cej.2016.05.034.

32. Feng M, Gao R, Staack D, Pillai SD, Sharma VK. Degradation of perfluoroheptanoic acid in water by electron beam irradiation. Environmental Chemistry Letters. 2021; 19(3):2689–94. https://doi.org/10.1007/s10311-021-01195-x

33. Lassalle J, Gao R, Rodi R, Kowald C, Feng M, Sharma VK, et al. Degradation of PFOS and PFOA in soil and groundwater samples by high dose Electron Beam Technology. Radiation Physics and Chemistry. 2021; 189:109705. https://doi.org/10.1016/j.radphyschem.2021.109705.

34. Londhe K, Lee C-S, Zhang Y, Grdanovska S, Kroc T, Cooper CA, et al. Energy Evaluation of Electron Beam Treatment of Perfluoroalkyl Substances in Water: A Critical Review. ACS ES&T Engineering. 2021; 1(5):827–41. https://doi.org/10.1021/acsestengg.0c00222

35. Zhang S, Lu X, Wang N, Buck RC. Biotransformation potential of 6:2 fluorotelomer sulfonate (6:2 FTSA) in aerobic and anaerobic sediment. Chemosphere. 2016; 154:224–30. https://doi.org/10.1016/j.chemosphere.2016.03.062 PMID: 27058914

36. Chen H, Choi YJ, Lee LS. Sorption, Aerobic Biodegradation, and Oxidation Potential of PFOS Alternatives Chlorinated Polyfluoroalkyl Ether Sulfonic Acids. Environmental Science & Technology. 2018; 52 (17):9827–34. https://doi.org/10.1021/acs.est.8b02913 PMID: 30099874

37. Huang S, Jaffé PR. Defluorination of Perfluorooctanoic Acid (PFOA) and Perfluorooctane Sulfonate (PFOS) by Acidimicrobium sp. Strain A6. Environmental Science & Technology. 2019; 53(19):11410–9. https://doi.org/10.1021/acs.est.9b04047 PMID: 31529965

38. Carter KE, Farrell J. Oxidative Destruction of Perfluorooctane Sulfonate Using Boron-Doped Diamond Film Electrodes. Environmental Science & Technology. 2008; 42(16):6111–5. https://doi.org/10.1021/es703273s PMID: 18767674

39. Choi JY, Lee Y-J, Shin J, Yang J-W. Anodic oxidation of 1,4-dioxane on boron-doped diamond electrodes for wastewater treatment. Journal of Hazardous Materials. 2010; 179(1):762–8. https://doi.org/10.1016/j.jhazmat.2010.03.067 PMID: 20381243

40. Liang S, Lin H, Yan X, Huang Q. Electro-oxidation of tetracycline by a Magnéli phase Ti4O7 porous anode: Kinetics, products, and toxicity. Chemical Engineering Journal. 2018; 332:628–36. https://doi.org/10.1016/j.cej.2017.09.109.

41. Shi H, Wang Y, Li C, Pierce R, Gao S, Huang Q. Degradation of Perfluorooctanesulfonate by Reactive Electrochemical Membrane Composed of Magnéli Phase Titanium Suboxide. Environmental Science & Technology. 2019; 53(24):14528–37. https://doi.org/10.1021/acs.est.9b04148 PMID: 31730354

42. Wang Y, Shi H, Pierce R, Huang Q. Electrochemical oxidation of perfluorooctanesulfonate (PFOS) on different porous Magneli phase titanium suboxides anodes. Abstr Pap Am Chem Soc. 2019;258.

43. Lin H, Xiao R, Xie R, Yang L, Tang C, Wang R, et al. Defect Engineering on a Ti4O7 Electrode by Ce3+ Doping for the Efficient Electrooxidation of Perfluorooctanesulfonate. Environmental Science & Technology. 2021; 55(4):2597–607. https://doi.org/10.1021/acs.est.0c06881 PMID: 33502168

44. Carrillo-Abad J, Pérez-Herranz V, Urtiaga A. Electrochemical oxidation of 6:2 fluorotelomer sulfonic acid (6:2 FTSA) on BDD: electrode characterization and mechanistic investigation. Journal of Applied Electrochemistry. 2018; 48(6):589–96. https://doi.org/10.1007/s10800-018-1180-8

45. Wang L, Lu J, Li L, Wang Y, Huang Q. Effects of chloride on electrochemical degradation of perfluorooctanesulfonate by Magnéli phase Ti4O7 and boron doped diamond anodes. Water Research. 2020; 170:115254. https://doi.org/10.1016/j.watres.2019.115254.

46. Zhuo Q, Luo M, Guo Q, Yu G, Deng S, Xu Z, et al. Electrochemical Oxidation of Environmentally Persistent Perfluorooctane Sulfonate by a Novel Lead Dioxide Anode. Electrochimica Acta. 2016; 213:358–67. https://doi.org/10.1016/j.electacta.2016.07.005.

47. Schaefer CE, Andaya C, Burant A, Condee CW, Urtiaga A, Strathmann TJ, et al. Electrochemical treatment of perfluorooctanoic acid and perfluorooctane sulfonate: Insights into mechanisms and application to groundwater treatment. Chemical Engineering Journal. 2017; 317:424–32. https://doi.org/10.1016/j.cej.2017.02.107.

48. Zhuo Q, Deng S, Yang B, Huang J, Wang B, Zhang T, et al. Degradation of perfluorinated compounds on a boron-doped diamond electrode. Electrochimica Acta. 2012; 77:17–22. https://doi.org/10.1016/j.electacta.2012.04.145.

49. Smith JR, Walsh FC, Clarke RL. Electrodes based on Magnéli phase titanium oxides: the properties and applications of Ebonex® materials. Journal of Applied Electrochemistry. 1998; 28(10):1021–33. https://doi.org/10.1023/A:1003469427858

50. Walsh FC, Wills RGA. The continuing development of Magnéli phase titanium sub-oxides and Ebonex® electrodes. Electrochimica Acta. 2010; 55(22):6342–51. https://doi.org/10.1016/j.electacta.2010.05.011.

51. You S, Liu B, Gao Y, Wang Y, Tang CY, Huang Y, et al. Monolithic Porous Magnéli-phase Ti4O7 for Electro-oxidation Treatment of Industrial Wastewater. Electrochimica Acta. 2016; 214:326–35. https://doi.org/10.1016/j.electacta.2016.08.037.

52. Lin H, Niu J, Liang S, Wang C, Wang Y, Jin F, et al. Development of macroporous Magnéli phase Ti4O7 ceramic materials: As an efficient anode for mineralization of poly- and perfluoroalkyl substances. Chemical Engineering Journal. 2018; 354:1058–67. https://doi.org/10.1016/j.cej.2018.07.210.

53. Asadi Zeidabadi F, Banayan Esfahani E, McBeath ST, Dubrawski KL, Mohseni M. Electrochemical degradation of PFOA and its common alternatives: Assessment of key parameters, roles of active species, and transformation pathway. Chemosphere. 2023; 315:137743. https://doi.org/10.1016/j.chemosphere.2023.137743 PMID: 36608884

54. Yang P, Wang Y, Lu J, Tishchenko V, Huang Q. Electrochemical Oxidation of Perfluorooctanesulfonate by Magnéli Phase Ti4O7 Electrode in the Presence of Trichloroethylene. Advances in Environmental and Engineering Research. 2020; 1(4):17. https://doi.org/10.21926/aeer.2004006

55. Martínez-Hincapié R, Wegner J, Anwar MU, Raza-Khan A, Franzka S, Kleszczynski S, et al. The determination of the electrochemically active surface area and its effects on the electrocatalytic properties of structured nickel electrodes produced by additive manufacturing. Electrochimica Acta. 2024; 476:143663. https://doi.org/10.1016/j.electacta.2023.143663.

56. Zhu P, Zhao Y. Cyclic voltammetry measurements of electroactive surface area of porous nickel: Peak current and peak charge methods and diffusion layer effect. Materials Chemistry and Physics. 2019; 233:60–7. https://doi.org/10.1016/j.matchemphys.2019.05.034.

57. Watzele S, Hauenstein P, Liang Y, Xue S, Fichtner J, Garlyyev B, et al. Determination of Electroactive Surface Area of Ni-, Co-, Fe-, and Ir-Based Oxide Electrocatalysts. ACS Catalysis. 2019; 9(10):9222–30. https://doi.org/10.1021/acscatal.9b02006

58. Ardizzone S, Fregonara G, Trasatti S. "Inner" and "outer" active surface of RuO2 electrodes. Electrochimica Acta. 1990; 35(1):263–7. https://doi.org/10.1016/0013-4686(90)85068-X.

59. Zhao W, Xing J, Chen D, Bai Z, Xia Y. Study on the performance of an improved Ti/SnO2-Sb2O3/PbO2 based on porous titanium substrate compared with planar titanium substrate. RSC Advances. 2015; 5(34):26530–9. https://doi.org/10.1039/C4RA13492C

60. Xu L, Scantlebury J. Electrochemical Surface Characterization of IrO2-Ta2O5 Coated Titanium Electrodes in Na2SO4 Solution. Journal of The Electrochemical Society. 2003; 150:B288–B93. https://doi.org/10.1149/1.1574033

61. Zhu P, Zhao Y. Effects of electrochemical reaction and surface morphology on electroactive surface area of porous copper manufactured by Lost Carbonate Sintering. RSC Advances. 2017; 7(42):26392–400. https://doi.org/10.1039/C7RA04204C

62. Dukhin AS, Goetz PJ. Chapter 2—Fundamentals of Interface and Colloid Science. In: Dukhin AS, Goetz PJ, editors. Characterization of Liquids, Dispersions, Emulsions, and Porous Materials Using Ultrasound (Third Edition): Elsevier; 2017. p. 19–83.

63. Mostafa E, Reinsberg P, Garcia-Segura S, Baltruschat H. Chlorine species evolution during electrochlorination on boron-doped diamond anodes: In-situ electrogeneration of Cl2, Cl2O and ClO2. Electrochimica Acta. 2018; 281:831–40. https://doi.org/10.1016/j.electacta.2018.05.099.

64. Wang Y, Pierce RD, Shi H, Li C, Huang Q. Electrochemical degradation of perfluoroalkyl acids by titanium suboxide anodes. Environmental Science: Water Research & Technology. 2020; 6(1):144–52. https://doi.org/10.1039/C9EW00759H

65. Wang Y, Li L, Wang Y, Shi H, Wang L, Huang Q. Electrooxidation of perfluorooctanesulfonic acid on porous Magnéli phase titanium suboxide Anodes: Impact of porous structure and composition. Chemical Engineering Journal. 2022; 431:133929. https://doi.org/10.1016/j.cej.2021.133929.

66. Wang F, Shih KM, Li XY. The partition behavior of perfluorooctanesulfonate (PFOS) and perfluorooctanesulfonamide (FOSA) on microplastics. Chemosphere. 2015; 119:841–7. https://doi.org/10.1016/j.chemosphere.2014.08.047 PMID: 25222623

67. Wang J, Wang S. Reactive species in advanced oxidation processes: Formation, identification and reaction mechanism. Chemical Engineering Journal. 2020; 401:126158. https://doi.org/10.1016/j.cej.2020.126158.

68. Ma J, Yang Y, Jiang X, Xie Z, Li X, Chen C, et al. Impacts of inorganic anions and natural organic matter on thermally activated persulfate oxidation of BTEX in water. Chemosphere. 2018; 190:296–306. https://doi.org/10.1016/j.chemosphere.2017.09.148 PMID: 28992483

69. Lide DR. CRC Handbook of Chemistry and Physics, 84th Edition: CRC Press LLC; 2004.

70. Yan S, Liu Y, Lian L, Li R, Ma J, Zhou H, et al. Photochemical formation of carbonate radical and its reaction with dissolved organic matters. Water Research. 2019; 161:288–96. https://doi.org/10.1016/j.watres.2019.06.002 PMID: 31202115

71. Behar D, Czapski G, Duchovny I. Carbonate radical in flash photolysis and pulse radiolysis of aqueous carbonate solutions. The Journal of Physical Chemistry. 1970; 74(10):2206–10. https://doi.org/10.1021/j100909a029

72. Joshi R, Mukherjee T. Carbonate radical anion-induced electron transfer in bovine serum albumin. Radiation Physics and Chemistry. 2006; 75(7):760–7. https://doi.org/10.1016/j.radphyschem.2005.12.040.

73. Phan Thi L-A, Do H-T, Lo S-L. Enhancing decomposition rate of perfluorooctanoic acid by carbonate radical assisted sonochemical treatment. Ultrasonics Sonochemistry. 2014; 21(5):1875–80. https://doi.org/10.1016/j.ultsonch.2014.03.027 PMID: 24751291

74. Phan Thi L-A, Do H-T, Lee Y-C, Lo S-L. Photochemical decomposition of perfluorooctanoic acids in aqueous carbonate solution with UV irradiation. Chemical Engineering Journal. 2013; 221:258–63. https://doi.org/10.1016/j.cej.2013.01.084.

75. Trojanowicz M, Bojanowska-Czajka A, Bartosiewicz I, Kulisa K. Advanced Oxidation/Reduction Processes treatment for aqueous perfluorooctanoate (PFOA) and perfluorooctanesulfonate (PFOS)–A review of recent advances. Chemical Engineering Journal. 2018; 336:170–99. https://doi.org/10.1016/j.cej.2017.10.153.

76. Black ED, Hayon E. Pulse radiolysis of phosphate anions H2PO4-, HPO42-, PO43-, and P2O74- in aqueous solutions. The Journal of Physical Chemistry. 1970; 74(17):3199–203. https://doi.org/10.1021/j100711a007

77. Mártire DO, Gonzalez MC. Aqueous Phase Kinetic Studies Involving Intermediates of Environmental Interest: Phosphate Radicals and Their Reactions with Substituted Benzenes. Progress in Reaction Kinetics and Mechanism. 2001; 26(2–3):201–18. https://doi.org/10.3184/007967401103165253

78. Rosso J A., Allegretti P E., Mártire D O., Gonzalez M C. Reaction of sulfate and phosphate radicals with α,α,α-trifluorotoluene. Journal of the Chemical Society, Perkin Transactions 2. 1999;(2):205–10. https://doi.org/10.1039/A807751G

79. Weiss E, Sáez C, Groenen-Serrano K, Cañizares P, Savall A, Rodrigo MA. Electrochemical synthesis of peroxomonophosphate using boron-doped diamond anodes. Journal of Applied Electrochemistry. 2008; 38(1):93–100. https://doi.org/10.1007/s10800-007-9405-2

80. Cañizares P, Sáez C, Sánchez-Carretero A, Rodrigo MA. Synthesis of novel oxidants by electrochemical technology. Journal of Applied Electrochemistry. 2009; 39(11):2143. https://doi.org/10.1007/s10800-009-9792-7

81. Crispim AC, da Silva Mendonça de Paiva S, de Araújo DM, Souza FL, Dos Santos EV. Ultrasound and UV technologies for wastewater treatment using boron-doped diamond anodes. Current Opinion in Electrochemistry. 2022; 33:100935. https://doi.org/10.1016/j.coelec.2021.100935.

82. Sánchez A, Llanos J, Sáez C, Cañizares P, Rodrigo MA. On the applications of peroxodiphosphate produced by BDD-electrolyses. Chemical Engineering Journal. 2013; 233:8–13. https://doi.org/10.1016/j.cej.2013.08.022.